Peer reviewed Journals
seron press

RESEARCH

Radial Thermal Legacy of Drilling Circulation in Early Drill Stem Testing of High-Temperature Wells

Wei Zhang,[1] Jun Li,[2] and Hao Chen[3]

[1] 采矿工程学院, 辽宁工程技术大学, 玉龙路 88 号, 阜新市, 辽宁省, 中国
[2] 资源与环境工程学院, 安徽理工大学, 舜耕中路 168 号, 淮南市, 安徽省, 中国
[3] 安全工程学院, 黑龙江科技大学, 松北大道 2468 号, 哈尔滨市, 黑龙江省, 中国

Abstract

Drilling circulation can leave a persistent temperature disturbance in the rock surrounding a wellbore, and that disturbance may remain active during the earliest stages of shut-in recovery, perforation, cleanup, and drill stem testing. In high-temperature wells the effect is especially important because the contrast between circulating fluid and undisturbed formation temperature is often large enough to create a substantial cooled near-wellbore region. When flow begins before that region has thermally recovered, the entering fluid does not represent the undisturbed reservoir state. Instead it carries the imprint of a radially distributed thermal disturbance whose magnitude and radial extent both evolve with time. The resulting bottom-hole pressure and temperature response is therefore shaped by hidden thermal recovery as well as by the hydraulic behavior of the test. This paper develops a technical framework for reconstructing that hidden radial thermal legacy and for linking it to early drill stem test interpretation. The formulation combines radial heat diffusion in the formation, transient interval entry conditions, temperature-dependent fluid-property effects, and reduced wellbore thermal transport. A compact state representation is introduced for the disturbed near-wellbore zone, and a pressure-temperature inversion is used to recover the hidden entry condition from observed test data. Particular attention is given to multirate tests, because changes in flow rate alter the radial weighting through which the hidden thermal field is sampled. The analysis derives the forward equations, the reduced inversion architecture, asymptotic observability results, and a field-oriented validation procedure designed to quantify entry-temperature bias, interval ambiguity, and uncertainty during the earliest portion of the test.

1. Introduction

A drill stem test performed soon after drilling does not begin from a neutral thermal state [1]. By the time the test starts, the wellbore and the adjacent formation have already experienced a prolonged exchange of heat associated with circulation. In a hot reservoir this exchange usually cools the rock around the wellbore. The disturbance is neither superficial nor instantaneous. It extends radially into the formation and then relaxes only slowly after circulation stops. When the time between the end of circulation and the start of flow is short, the earliest produced fluid must cross a formation annulus whose temperature remains below the undisturbed formation value [2]. The first fluid seen by the wellbore is therefore conditioned by a hidden thermal legacy of drilling.

That observation matters because early drill stem test interpretation is commonly built around the assumption that measured pressure and temperature respond to hydraulic drawdown from an approximately undisturbed reservoir. The hidden thermal state violates that assumption in a specific way. It changes the temperature of the fluid entering the wellbore. In doing so it modifies fluid properties and alters the connection between interval inflow and measured wellbore response. Under some conditions the distortion is small enough to ignore [3]. Under other conditions, especially in high-temperature wells or after short shut-in periods, the distortion is large enough that equilibrium-based interpretation produces systematic bias.

The problem is not simply that the entering temperature is shifted from the undisturbed formation temperature. The more difficult issue is that the shift is time dependent and nonlocal. The fluid entering the wellbore at any moment is not influenced by one point in the formation. It is influenced by a radial region whose thermal state has been shaped by prior circulation and is sampled through a flow-dependent weighting. Early in the flow period, the sampled region is concentrated very close to the wellbore [4]. Later, the sampled region broadens. If the test contains multiple flow rates, the weighting changes again with each rate change. Therefore the same hidden radial field generates different interval entry conditions as the test

Table 1. Physical processes influencing early drill stem testing after drilling circulation

Process	Physical Mechanism	Time Scale	Impact on Test Response
Circulation cooling	Heat removal by drilling fluid	Hours–days	Creates cooled near-wellbore zone
Radial heat diffusion	Thermal recovery in formation	Hours–weeks	Gradual temperature restoration
Wellbore heat exchange	Rock–fluid thermal transfer	Minutes–hours	Alters bottom-hole temperature
Multirate sampling	Rate-dependent radial inflow	Minutes–hours	Changes thermal weighting of inflow

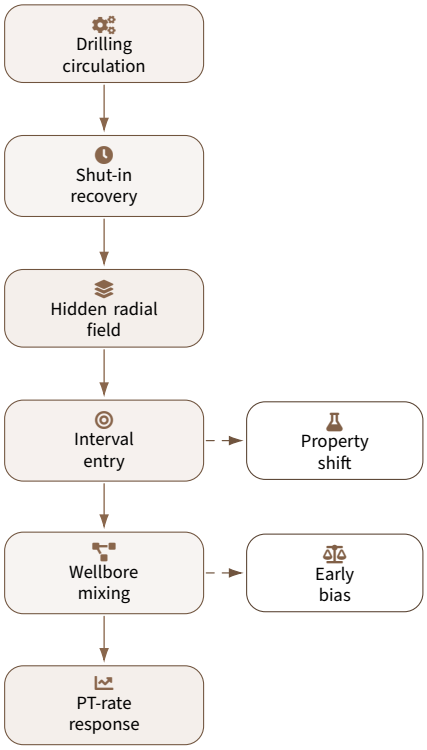


Figure 1. Causal structure of the problem. Drilling circulation creates a cooled near-wellbore disturbance, shut-in only partly relaxes it, and the remaining hidden radial field controls interval entry temperature during the earliest flow period. The resulting wellbore pressure–temperature response therefore carries both hydraulic information and a persistent thermal memory.

proceeds. Any realistic interpretation of early temperature and rate must respect that nonlocal structure.

A second layer of difficulty arises in multilayer completions or in perforated intervals with nonuniform contribution. Distinct entry zones may carry distinct thermal histories because the circulation environment, local rock properties, and shut-in recovery times can vary across the interval [5]. The mixed wellbore signal may then combine several hidden entry temperatures. A model that treats the entire interval as a single uniform thermal source can fit the measured temperature only by absorbing interval-scale structure into effective parameters. Such a fit may appear numerically satisfactory while remaining physically misleading.

The present work proceeds from the view that early drill stem test interpretation in recently circulated wells should be cast as a problem of reconstructing a hidden radial temperature field from its pressure-temperature consequences. The field is not directly measured, but it is not arbitrary either [6]. It is produced by a specific thermal forcing history during circulation, evolves under heat diffusion after circulation ends, and influences the test through a structured sequence of operators. The first operator maps circulation history to the radial thermal disturbance in the formation. The second maps that hidden radial disturbance to interval entry temperature through flow-weighted sampling. The third maps the interval entry conditions to measured bottom-hole temperature through mixing and wellbore transport. Pressure enters the same chain through interval inflow, fluid properties, and rate allocation. The inverse problem is therefore to estimate the hidden ra-

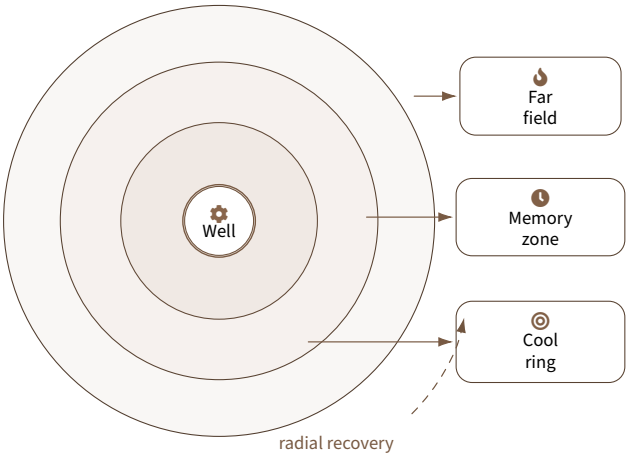


Figure 2. Radial thermal legacy around the tested well. The strongest cooling persists closest to the wellbore, while a broader but weaker memory zone extends outward into the formation. During early drill stem testing the inflow first encounters the inner cooled ring, so the entering fluid temperature can remain substantially below the undisturbed far-field temperature.

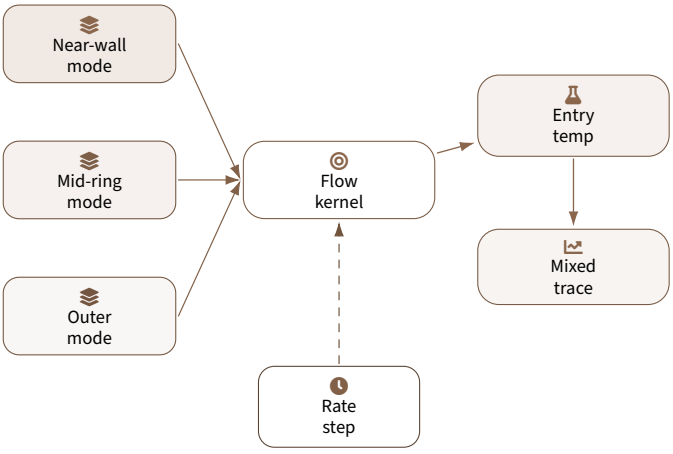


Figure 3. Flow-weighted sampling of the hidden radial temperature field. The interval entry temperature is not tied to one radius; it is a weighted projection of near-wall, intermediate, and broader thermal modes. Rate changes alter the projection kernel, so the same hidden field can produce different entry conditions at different stages of a multirate test.

dial thermal state and selected uncertain transport parameters from the measured pressure-temperature-rate response [7].

The practical relevance of this physical setting is consistent with the near-wellbore cooling analysis of Hasan et al. (2024) [8], who showed that circulation-induced thermal disturbance can materially affect fluid-entry temperature and early drill stem test behavior. The approach developed here stays within that same field context but emphasizes a different technical target. The main task is not to forward-predict one temperature trace from one assumed thermal profile. The main task is to reconstruct the hidden radial state itself in a way that is stable, physically constrained, and useful for entry-condition interpretation.

This requires careful mathematical design [9]. The hidden radial field must be represented compactly enough for inversion yet richly enough to preserve the near-wall thermal deficit that dominates early entry conditions. The wellbore model must be reduced enough for repeated evaluation but still retain interval mixing and heat exchange. The inversion must use both pressure and temperature because either channel alone leaves important ambiguities unresolved. The regularization must encode diffusion-like evolution, because the radial thermal field is only partially observable from early test data. A model that neglects these constraints may fit the measured temperature locally while inventing a thermal history that could not have arisen from circulation and recovery.

The sections that follow are organized around the causal structure of the physical problem rather than around a generic model template [10]. The next section begins with the thermal aftermath of circulation, because that is where the hidden state originates. The following section examines how flow samples that hid-

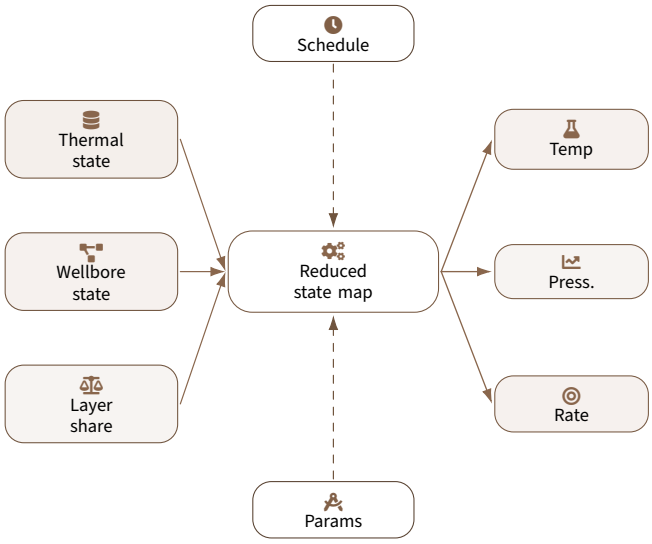


Figure 4. Reduced coupled model used for interpretation. Hidden thermal memory, reduced wellbore transport, and interval contribution variables are gathered into a compact state representation. Test schedule and uncertain parameters modulate the same state map, which then generates the observed temperature, pressure, and rate channels.

Table 2. Symbols and primary variables used in the thermal recovery formulation

Symbol	Definition	Units
r	Radial distance from well axis	m
T_∞	Undisturbed formation temperature	°C
$\theta(r,t)$	Formation temperature disturbance	°C
α	Thermal diffusivity	m^2/s
k_e	Effective thermal conductivity	W/(m • K)
$(\rho c)_e$	Effective volumetric heat capacity	J/(m^3 • K)

den state and turns it into interval entry temperature. Only after that mapping is explicit does the paper introduce the reduced wellbore response and the inverse problem. Later sections analyze observability and bias pathways, then turn to implementation and validation. The argument remains technical throughout, but the central idea is simple: early drill stem test data in recently circulated wells are best interpreted as filtered observations of a recovering radial thermal field rather than as direct expressions of a thermally undisturbed reservoir.

2. Thermal Aftermath of Circulation

Let r denote radial distance from the well axis, r_w the effective wellbore or completion radius, and r_b an outer radius beyond which the circulation-induced disturbance is negligible over the operational time window [11]. Let T_∞ be the undisturbed formation temperature at the tested interval. The disturbed formation temperature is written as

$$\theta(r,t) = T_f(r,t) - T_\infty, \tag{1}$$

where $T_f(r,t)$ is the local formation temperature. In the common case of a hot reservoir exposed to cooler circulating fluid, $\theta(r,t)$ is negative near the wellbore at the end of circulation.

The starting point after circulation is a radial heat-recovery problem [12]. Under effective local thermal equilibrium between the porous matrix and the resident fluid, a reduced radial energy balance can be written as

$$(\rho c)_e \frac{\partial \theta}{\partial t} = \frac{1}{r}\frac{\partial}{\partial r}\left(k_e r \frac{\partial \theta}{\partial r}\right) + q_w(r,t), \tag{2}$$

where $(\rho c)_e$ is the effective volumetric heat capacity of the formation-fluid system, k_e is effective thermal conductivity, and $q_w(r,t)$ is a residual source term representing remaining wellbore-related thermal interaction after circulation has ceased. The corresponding diffusivity is $\alpha = k_e/(\rho c)_e$.

The state at the end of circulation is itself the result of a thermal forcing history. If the effective heat-transfer history imposed at the wellbore is represented by $q_c(\tau)$ over $0 \le \tau \le t_c$, where t_c is the end of circu-

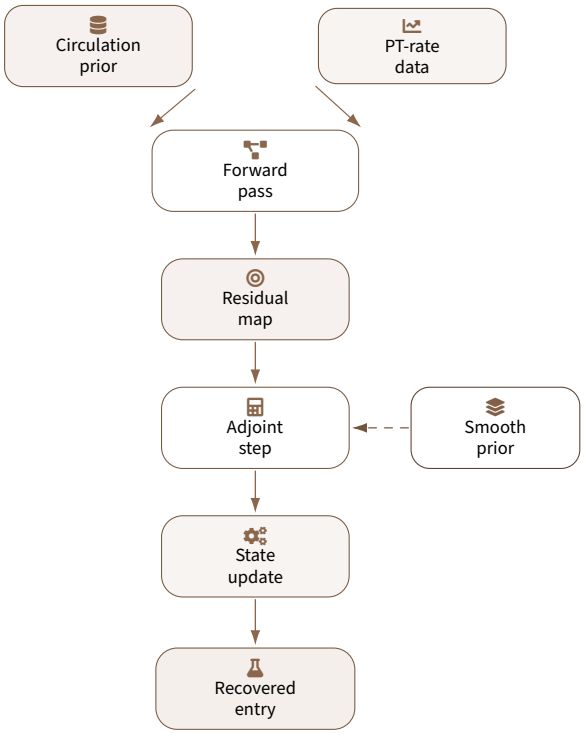


Figure 5. Integrated reconstruction workflow. Prior information inherited from circulation history is fused with measured pressure–temperature–rate data through repeated forward evaluation, residual formation, adjoint sensitivity propagation, and state updates. The output is a physically constrained estimate of hidden entry conditions rather than a purely empirical fit to the observed traces.

Table 3. Stages of thermal evolution around the wellbore

Stage	Dominant Process	Temperature Trend	Interpretation Implication
Active circulation	Forced cooling	Rapid decline near well	Strong disturbance created
Immediate shut-in	Diffusion dominated	Slow recovery begins	Entry temperature biased
Early flow	Radial sampling	Non-uniform inflow temperature	Test interpretation affected
Late recovery	Thermal equilibrium approach	Gradual stabilization	Bias reduces

lation, then a line-source style representation yields

$$\theta(r,t) = -\int_0^{t_c} \frac{q_c(\tau)}{4\pi k_e H} E_1\left(\frac{r^2}{4\alpha(t-\tau)}\right) d\tau, \quad t > t_c, \tag{3}$$

where H is an effective interval thickness and E_1 is the exponential integral [13]. This expression is useful not because it is exact in every completion geometry, but because it makes the memory structure explicit. The disturbed near-wellbore state present during testing is a weighted integral of prior circulation history filtered through radial diffusion.

The thermal aftermath is therefore best interpreted as a hidden memory field rather than as a boundary perturbation of negligible duration. The degree to which that field matters at the start of testing depends on shut-in duration. Let t_f denote the start of flow. A simple diffusion scaling shows that the radial disturbance radius evolves roughly as [14]

$$r_d(t) \sim \sqrt{4\alpha(t-t_c)}. \tag{4}$$

At the same time, the amplitude decays with increasing time. A longer shut-in reduces the near-wall temperature deficit but also broadens the region over which the residual thermal signal is distributed. These two changes influence early test interpretation differently. The near-wall deficit controls the strongest entry-temperature bias. The broader residual field affects later-time entry weighting.

A wellbore that is shut in after circulation may continue to exchange heat with the surrounding rock [15]. That interaction can be expressed through a mixed

Table 4. Reduced-state representation of the disturbed thermal field

Component	Mathematical Form	Physical Meaning	Role in Model
Basis function $\phi_i(r)$	Radial mode shape	Spatial thermal structure	Captures disturbance geometry
Coefficient $a_i(t)$	Modal amplitude	Strength of disturbance	Hidden thermal state
Decay rate λ_i	Modal relaxation constant	Diffusive recovery speed	Governs temporal evolution
Wall forcing $f_i^w(t)$	Boundary interaction term	Wellbore heat influence	Drives near-wall dynamics

Table 5. Factors controlling interval entry temperature during flow

Factor	Description	Mathematical Role	Effect on Inflow
Radial weighting $w(r,t)$	Flow sampling kernel	Entry operator integral	Selects thermal region
Thermal disturbance $\theta(r,t)$	Residual cooling field	State variable	Alters entry temperature
Flow rate	Operational control variable	Modifies weighting kernel	Changes sampling radius
Interval heterogeneity	Layer-specific properties	Interval-dependent coefficients	Produces mixed inflow

thermal boundary condition at $r = r_w$,

$$-k_e \left.\frac{\partial \theta}{\partial r}\right|_{r=r_w} = h_w^* \left(\theta(r_w,t) - \theta_w(t)\right), \tag{5}$$

where h_w^* is an effective wall conductance and $\theta_w(t) = T_w(t) - T_\infty$ is the wellbore temperature disturbance. This boundary condition matters because the hidden radial field at the start of flow is influenced not only by the circulation forcing but also by the shut-in evolution of the wellbore column itself.

To prepare the model for inversion, the hidden radial field is projected onto a reduced basis $\{\phi_i(r)\}_{i=1}^M$,

$$\theta(r,t) = \sum_{i=1}^{M} a_i(t)\phi_i(r). \tag{6}$$

The coefficients $a_i(t)$ are the reduced thermal-memory state. If the basis is chosen to align with radial diffusion, then their evolution during shut-in is approximately

$$\dot{a}_i(t) = -\lambda_i a_i(t) + f_i^w(t) + n_i(t), \tag{7}$$

where λ_i are modal decay rates, $f_i^w(t)$ represents wall-related forcing, and $n_i(t)$ is a correction term capturing unresolved effects. The first modes correspond to near-wall structure, while later modes capture broader radial recovery.

This reduced representation already reveals an important identifiability hierarchy [16]. The near-wall modes evolve rapidly and most strongly affect the earliest entry conditions. The broader modes decay more slowly but are less visible in the earliest flow measurements. The test therefore carries different levels of information about different parts of the hidden thermal state. Any inversion that pretends otherwise will overstate what the data actually reveal.

3. How Flow Samples the Hidden Thermal State

The fluid that enters the wellbore does not come from a single temperature at a single radius [17]. It samples the radial thermal field through a flow-dependent weighting that evolves in time. That weighting is the mechanism by which hidden thermal memory becomes operationally visible.

For interval ℓ, let $w_\ell(r,t)$ denote the radial entry-weighting kernel. The corresponding interval entry temperature is

$$T_{\mathrm{in},\ell}(t) = T_{\infty,\ell} + \frac{\int_{r_{w,\ell}}^{r_{b,\ell}} w_\ell(r,t)\theta_\ell(r,t)\,dr}{\int_{r_{w,\ell}}^{r_{b,\ell}} w_\ell(r,t)\,dr}. \tag{8}$$

The kernel $w_\ell(r,t)$ can be interpreted as a mass-flux or residence-time weighting derived from the local inflow field. What matters for the present analysis is that it changes with time and with rate [18].

Substituting the reduced thermal representation yields

$$T_{\mathrm{in},\ell}(t) = T_{\infty,\ell} + \sum_{i=1}^{M_\ell} c_{\ell,i}(t)a_{\ell,i}(t), \tag{9}$$

where

$$c_{\ell,i}(t) = \frac{\int_{r_{w,\ell}}^{r_{b,\ell}} w_\ell(r,t)\phi_{\ell,i}(r)\,dr}{\int_{r_{w,\ell}}^{r_{b,\ell}} w_\ell(r,t)\,dr}. \tag{10}$$

The vector $c_\ell(t)$ is the entry operator for interval ℓ. It converts the hidden thermal coefficients into the thermodynamic condition of fluid arriving at the wellbore.

Table 6. Observation channels used for reconstruction of hidden thermal states

Measurement	Information Provided	Interpretation Role
Bottom-hole temperature	Mixed wellbore thermal response	Detects entry temperature changes
Bottom-hole pressure	Hydraulic drawdown signal	Constrains inflow dynamics
Total flow rate	Operational boundary condition	Determines inflow weighting
Rate changes	Dynamic sampling variation	Improves thermal observability

Table 7. Key components of the reduced wellbore thermal transport model

Term	Representation	Physical Interpretation	Influence on Measurements
Convective transport	$\dot{m}h$ term	Axial heat movement in wellbore	Delays entry signal
Wall heat transfer	$UP(T_f - T_w)$	Rock–fluid heat exchange	Smooths temperature profile
Interval enthalpy input	$\dot{m}_\ell h_\ell^{in}$	Layer inflow energy	Generates mixed temperature
Axial correction Q_a	Reduced residual term	Minor transport effects	Adjusts local balance

At very early times after flow begins, the kernel is concentrated near the wellbore. The interval entry temperature therefore depends mainly on a small number of near-wall thermal coefficients:

$$T_{\mathrm{in},\ell}(t) = T_{\infty,\ell} + \sum_{i=1}^{m_e} c_{\ell,i}^{(e)}(t) a_{\ell,i}(t) + \mathcal{O}(\epsilon_t), \qquad (11)$$

where $m_e \ll M_\ell$ [19]. This early-time asymptotic relation explains why the strongest entry-temperature bias is often recoverable from early data even when the full radial thermal field is not. The hidden radial profile has more degrees of freedom than the earliest inflow can observe, but the portion of the profile that matters most for immediate entry condition is precisely the portion closest to the wellbore.

Rate changes alter the entry operator even when the hidden coefficients remain continuous. If a multirate test changes from one rate level to another at time t_r, then

$$\Delta T_{\mathrm{in},\ell} = T_{\mathrm{in},\ell}(t_r^+) - T_{\mathrm{in},\ell}(t_r^-) \approx \left(c_\ell^+ - c_\ell^-\right)^\top a_\ell(t_r). \qquad (12)$$

The hidden thermal state is therefore observed through multiple projections over the course of a multirate test. This is one reason multirate data can improve thermal reconstruction rather than merely complicate it [20].

A multilayer completion adds another level of nonlocality. If the tested interval is represented by L entries, then each interval has its own hidden thermal coefficients $a_\ell(t)$ and its own entry operator $c_\ell(t)$. The interval entry temperatures may differ even when their far-field formation temperatures are similar, simply because their circulation histories and shut-in recoveries differed. This distinction can be important when early mixed wellbore temperature is used to infer interval contribution.

The interval entry bias [21]

$$\Delta T_\ell(t) = T_{\infty,\ell} - T_{\mathrm{in},\ell}(t) \qquad (13)$$

is the most direct measure of thermal distortion in the early inflow. It also determines the first-order error that would arise if equilibrium-entry assumptions were imposed. If a fluid property χ entering the inflow law depends on temperature, then

$$\chi(T_{\mathrm{in},\ell}) \approx \chi(T_{\infty,\ell}) - \chi_T(T_{\infty,\ell})\Delta T_\ell. \qquad (14)$$

This means that hidden thermal memory affects flow interpretation not only through the temperature channel but also through temperature-dependent property shifts inside the hydraulic model.

The entry operator is therefore the core nonlocal bridge between the hidden formation state and the measurable test response. The next section shows how interval entry conditions are transported and mixed in the wellbore to generate the observed pressure-temperature response [22].

4. Reduced Wellbore Response and Mixed Observation Generation

Measured bottom-hole temperature is not identical to interval entry temperature. By the time the fluid reaches the measurement point, interval streams have mixed and the wellbore has exchanged heat with the surrounding formation. The wellbore therefore acts as a transport operator between hidden interval entry conditions and observed temperature.

Let $T_w(z,t)$ be the wellbore fluid temperature. A

Table 8. Main components of the inverse reconstruction framework

Component	Function	Mathematical Element	Purpose
Forward model	Simulates test response	$\mathcal{F}, \mathcal{H}$ operators	Predicts measurements
State trajectory	Hidden thermal evolution	$x_{0:N}$	Represents memory field
Regularization	Physical constraints	$\mathcal{R}$ terms	Stabilizes inversion
Adjoint gradient	Sensitivity computation	Lagrange multipliers	Efficient optimization

Table 9. Evaluation metrics for validating reconstructed entry conditions

Metric	Definition	Purpose	Interpretation
Entry temperature error	Difference between true and estimated T_{in}	Assess thermal reconstruction	Lower values indicate accuracy
Rate bias	Deviation from true flow rate	Detect interpretation distortion	High bias implies thermal impact
Interval ambiguity	Uncertainty in contribution factors	Identify poorly constrained zones	Indicates need for additional data
Consistency check	Agreement with circulation history	Validate physical plausibility	Ensures realistic solution

reduced energy balance is

$$\begin{aligned}\frac{\partial}{\partial t}\left(\rho_w A_w c_{p,w} T_w\right) + \frac{\partial}{\partial z}\left(\dot{m} h_w\right) &= U(z,t)P(z) \\ &\cdot \left(T_f(r_w^+, z, t) - T_w(z,t)\right) \\ &+ \sum_{\ell=1}^{L} \dot{m}_\ell(t) h_\ell^{\mathrm{in}}(t)\delta(z - z_\ell) \\ &+ Q_a(z,t). \end{aligned} \tag{15}$$

where $h_\ell^{\mathrm{in}}(t)$ is the interval entry enthalpy implied by $T_{\mathrm{in},\ell}(t)$, U is the wall conductance, and Q_a collects reduced axial effects. The wellbore temperature field is projected onto axial basis functions: [23]

$$T_w(z,t) = \bar{T}_w(z) + \sum_{j=1}^{N_b} b_j(t)\psi_j(z). \tag{16}$$

The coefficient vector $b(t)$ is the reduced wellbore thermal state.

The measured bottom-hole temperature then takes the form

$$T_{bh}(t) = \mathcal{W}\left(b(t), \{\dot{m}_\ell(t)\}_{\ell=1}^{L}, \{T_{\mathrm{in},\ell}(t)\}_{\ell=1}^{L}, u(t)\right). \tag{17}$$

This operator $\mathcal{W}$ is distinct from the entry operator. It acts after interval entry conditions are formed, and it determines how quickly those entry conditions appear in the measured channel.

The pressure channel is described by a reduced interval inflow law. For interval ℓ,

$$\dot{m}_\ell(t) = \mathcal{Q}_\ell\left(p_{r,\ell}, p_{bh}(t), T_{\mathrm{in},\ell}(t), \kappa_\ell(t)\right), \tag{18}$$

where $p_{r,\ell}$ is an effective interval pressure and $\kappa_\ell(t)$ is a reduced contribution factor. The temperature dependence enters through fluid properties and possibly through interval correction terms [24]. Hence the hidden thermal state influences both the temperature and pressure channels, though by different mechanisms.

A convenient parametrization of interval contribution is

$$\dot{m}_\ell(t) = \dot{m}_{\mathrm{tot}}(t)\frac{\exp(\zeta_\ell(t))}{\sum_{j=1}^{L}\exp(\zeta_j(t))}, \tag{19}$$

where $\zeta_\ell(t)$ are interval allocation variables. These variables influence temperature by controlling the mixture of interval entry enthalpies and influence pressure by controlling distributed inflow. In other words, the same hidden contribution structure is visible in both channels.

The reduced hidden state is therefore [25]

$$x_k = \left[a_{1,k}^\top, \ldots, a_{L,k}^\top, b_k^\top, \zeta_k^\top, \vartheta_k^\top\right]^\top, \tag{20}$$

and the reduced dynamics become

$$x_{k+1} = A_{\sigma_k}(\vartheta_k)x_k + B_{\sigma_k}(\vartheta_k)u_k + r_{\sigma_k}(x_k, u_k, \vartheta_k) + \epsilon_k. \tag{21}$$

The observation vector is

$$y_k = \begin{bmatrix} T_{bh,k} \\ p_{bh,k} \\ q_k \end{bmatrix} = \mathcal{H}_{\sigma_k}(x_k, u_k, \vartheta_k) + \eta_k. \tag{22}$$

The mode σ_k identifies shut-in, drawdown, buildup, or another operational segment. The hidden thermal state remains continuous across those changes, while the observation map changes because the test schedule changes how the hidden state is sampled.

This reduced structure is the forward model used by the inversion [26]. It keeps the thermal memory explicit and locates the entry-condition map between

formation and wellbore rather than collapsing them into one empirical correction. The next section turns this forward map into a reconstruction procedure.

5. Integrated Reconstruction of Hidden Entry Conditions

The inverse problem is to reconstruct hidden thermal memory, interval contributions, and uncertain parameters from measured pressure, temperature, and rate. Let $x_{0:N}$ denote the hidden state trajectory and ϑ the parameter vector over a test window. The reduced forward model is the nonlinear map

$$\begin{aligned} x_{k+1} &= \mathcal{F}_k(x_k, u_k, \vartheta) \\ y_k &= \mathcal{H}_k(x_k, u_k, \vartheta). \end{aligned} \tag{23}$$

A regularized reconstruction functional is

$$\begin{aligned} \mathcal{J}(x_{0:N}, \vartheta) = {} & \frac{1}{2}\sum_{k=0}^{N}\Big(y_k - \mathcal{H}_k(x_k, u_k, \vartheta)\Big)^{\top} R_k^{-1} \\ & \cdot \Big(y_k - \mathcal{H}_k(x_k, u_k, \vartheta)\Big) \\ & + \frac{1}{2}\sum_{k=0}^{N-1}\Big(x_{k+1} - \mathcal{F}_k(x_k, u_k, \vartheta)\Big)^{\top} Q_k^{-1} \\ & \cdot \Big(x_{k+1} - \mathcal{F}_k(x_k, u_k, \vartheta)\Big) \\ & + \frac{1}{2}(x_0 - m_0)^{\top} P_0^{-1}(x_0 - m_0) \\ & + \frac{1}{2}(\vartheta - \vartheta_0)^{\top} W^{-1}(\vartheta - \vartheta_0) \\ & + \mathcal{R}(x_{0:N}, \vartheta). \end{aligned} \tag{24}$$

The prior mean m_0 and covariance P_0 carry information from the circulation history into the test interpretation [27]. Without that inheritance, broad thermal modes would be weakly constrained. The parameter prior (ϑ_0, W) regularizes diffusivities, conductances, and correction factors.

A specifically thermal regularization term is

$$\mathcal{R}_a = \lambda_a \sum_{\ell=1}^{L}\sum_{k=0}^{N-1} \left|0 a_{\ell,k+1} - G_{\ell,k}(\vartheta)\, a_{\ell,k}\right| 0_2^2, \tag{25}$$

where $G_{\ell,k}(\vartheta)$ is the nominal reduced recovery propagator. A contribution regularizer is

$$\mathcal{R}_\zeta = \lambda_\zeta \sum_{k=0}^{N-1} |0\zeta_{k+1} - \zeta_k| 0_2^2. \tag{26}$$

Additional parameter penalties enforce admissible conductance and diffusivity ranges.

Adjoint gradients make the optimization tractable [28]. Introducing multipliers λ_{k+1} for the dynamic constraints yields the backward recursion

$$\lambda_N = \left(\partial_{x_N}\mathcal{H}_N\right)^{\top} R_N^{-1}\left(y_N - \mathcal{H}_N\right), \tag{27}$$

and for $k = N-1, \ldots, 0$,

$$\begin{aligned} \lambda_k = {} & \left(\partial_{x_k}\mathcal{F}_k\right)^{\top} Q_k^{-1}\left(x_{k+1} - \mathcal{F}_k\right) + \left(\partial_{x_k}\mathcal{H}_k\right)^{\top} R_k^{-1}\left(y_k - \mathcal{H}_k\right) \\ & + \left(\partial_{x_k}\mathcal{F}_k\right)^{\top}\lambda_{k+1} - \partial_{x_k}\mathcal{R}. \end{aligned} \tag{28}$$

The parameter gradient is

$$\begin{aligned} \nabla_\vartheta \mathcal{J} = {} & W^{-1}(\vartheta - \vartheta_0) + \nabla_\vartheta \mathcal{R} - \sum_{k=0}^{N}\left(\partial_\vartheta \mathcal{H}_k\right)^{\top} R_k^{-1}\left(y_k - \mathcal{H}_k\right) \\ & - \sum_{k=0}^{N-1}\left(\partial_\vartheta \mathcal{F}_k\right)^{\top} Q_k^{-1}\left(x_{k+1} - \mathcal{F}_k\right) - \sum_{k=0}^{N-1}\left(\partial_\vartheta \mathcal{F}_k\right)^{\top}\lambda_{k+1}. \end{aligned} \tag{29}$$

The sensitivity of the temperature channel to the hidden thermal memory is mediated by the entry operator:

$$\frac{\partial T_{\mathrm{in},\ell,k}}{\partial a_{\ell,k}} = c_{\ell,k}. \tag{30}$$

This relation is the core of the reconstruction. It makes explicit that the data never observe the hidden thermal coefficients directly. They observe only the projections created by $c_{\ell,k}$, and those projections change with the rate schedule. The inversion must therefore preserve both the continuity of the hidden thermal state and the time dependence of the entry operator [29].

A receding-window implementation is natural for field use. Each new block of data updates the most recent state trajectory and refines the hidden thermal coefficients before the next operational change. A full post-test run can then smooth the solution over the entire horizon. In both cases the same principle applies: the hidden thermal memory created during circulation is carried into the test as a structured latent state and reconstructed from its pressure-temperature consequences rather than from temperature alone.

6. Field-Oriented Evaluation and Practical Reading of Results

A meaningful evaluation of this framework should focus on the quantities that alter interpretation, not only on goodness of fit of the observed traces. In synthetic cases where the hidden state is known, the first diagnostic quantity is the interval entry temperature [30]. Let $T^{\star}_{\mathrm{in},\ell,k}$ denote the true interval entry temperature and $\hat{T}_{\mathrm{in},\ell,k}$ its reconstruction. A weighted early-time error is

$$\mathcal{E}_{\mathrm{entry},\ell} = \frac{\sum_{k\in\mathcal{I}_f}\omega_k\left(T^{\star}_{\mathrm{in},\ell,k} - \hat{T}_{\mathrm{in},\ell,k}\right)^2}{\sum_{k\in\mathcal{I}_f}\omega_k}, \tag{31}$$

where the weights emphasize the earliest flow period. This metric is more relevant than full-profile error because the entry condition is the quantity that drives the interpretation bias.

The second diagnostic quantity is the interval or total rate bias induced by ignoring hidden thermal memory. If $q_k^\star$ is the true rate and q_k^{eq} is the rate inferred under equilibrium-entry assumptions, then

$$\mathcal{B}_q = \frac{1}{N_f} \sum_{k \in \mathcal{I}_f} \left(q_k^\star - q_k^{\mathrm{eq}} \right)^2 . \tag{32}$$

Comparing this with the rate error under the thermal-memory inversion shows directly whether explicit reconstruction of entry conditions changes the interpretation in a practically meaningful way [31].

The third diagnostic quantity is interval ambiguity. In multilayer cases the inversion should report uncertainty on the interval contribution variables ζ_ℓ and on interval-specific entry temperatures rather than only on the total mixed response. If the posterior or inverse-Hessian approximation remains broad for a given interval, then the data do not strongly identify that interval' s hidden thermal state. This distinction between total-response fit and interval-level identifiability is essential in field applications.

For field cases, hidden truth is unavailable. The evaluation must therefore proceed by consistency checks [32]. One asks whether the reconstructed hidden thermal memory is compatible with the known circulation duration, thermal contrast, and shut-in time. One asks whether equilibrium-entry assumptions produce unexplained early-time temperature-pressure mismatch that disappears once hidden thermal memory is admitted. One asks whether the resulting interval contributions remain physically plausible. A successful reconstruction does not merely fit temperature. It makes the temperature, pressure, and operational history agree within one coherent thermohydraulic account.

The framework also provides a practical criterion for when the extra complexity is justified [33]. If the reconstructed entry-temperature bias is small relative to uncertainty, then the well may already be close enough to thermal equilibrium for simpler models to suffice. If the reconstructed bias is large and strongly supported by the data, then equilibrium-entry interpretation is unsafe during the early portion of the test. The method is therefore not an all-or-nothing replacement for existing analysis. It is a way to decide whether hidden thermal memory is still active enough to matter.

7. Conclusion

Early drill stem test data in recently circulated wells are generated by a system that has not forgotten its thermal past. The near-wellbore region retains a radial temperature disturbance created during circulation, and that disturbance shapes the temperature of fluid entering the wellbore during the earliest stages of flow [34]. Because the entry condition is itself hidden and is seen only through changing flow-weighted projections, the interpretation problem is naturally one of nonlocal thermal memory inversion rather than local boundary correction.

The framework developed here represented that memory in reduced radial coordinates, mapped it into interval entry temperatures through a time-dependent entry operator, and coupled those entry conditions to a reduced pressure-temperature wellbore response. From that structure, an integrated inverse reconstruction over thermal coefficients, interval contributions, and uncertain parameters was derived. The analysis showed why the earliest data constrain near-wall thermal deficit most strongly, why multirate schedules improve thermal observability by changing the projection geometry, and why broad radial modes remain partly prior supported even when the observed fit is good. The practical result is a more disciplined way to decide when hidden thermal recovery matters for early drill stem test interpretation and how strongly it affects inferred entry conditions and early flow behavior. In wells where the disturbed near-wellbore zone has not yet recovered, a nonlocal thermal-memory model provides a firmer basis for interpretation than equilibrium-entry assumptions or scalar temperature corrections alone [35].

References

[1] E. Gras and W. Ott, "Designing, planning nitrogen jobs. part 1. flow back, commingled n/sub 2/ fluid curves aid planning," Oil & Gas Journal, 2 1979.

[2] M. Sippel, "Improved recovery demonstration for williston basin carbonates. final report," 7 1998.

[3] H. V. Vu and L. Cao, "On the appraisal and development of st-x field: uncertainties and challenges," Science and Technology Development Journal, vol. 17, pp. 110–116, 9 2014.

[4] W. Weiss, J. Buckley, and A. Ouenes, "Integration of advanced geoscience and engineering techniques to quantify interwell heterogeneity in reservoir models. final report, september 29, 1993–september 30, 1996," 5 1997.

[5] T. M. Susantoro, S. Suliantara, H. L. Setiawan, B. Widarsono, and K. Wikantika, "Heavy oil potentials in central sumatra basin, indonesia using remote sensing, gravity, and petrophysics data: From literature review to interpretations and analyses," Indonesian Journal of Science and Technology, vol. 7, pp. 363–384, 10 2022.

[6] M. Santamaria, R. Roberts, and S. Gill, "Evaluation of paraffin deposition potential using drillstem test fluids," in SPE Production Operations Symposium, SPE, 4 1991.

[7] M. Gibson, S. Mazumder, P. Probst, and M. Scott, "Application of open-hole diagnostic fracture injection test results to regional stress interpretation in bowen basin coals," in SPE Unconventional Resources Conference and Exhibition-Asia Pacific, SPE, 11 2013.

[8] A. R. Hasan, K. Manikonda, M. Jang, M. A. Rahman, and G. Hashmi, "Estimating near-wellbore cooling due to drilling circulation and its effect on drill stem test," in SPE Annual Technical Conference and Exhibition?, p. D021S015R003, SPE, 2024.

[9] A. H. Abbas, W. R. W. Sulaiman, M. Z. Jaafar, and A. A. Aja, "Transient pressure analysis for vertical oil exploration wells: a case of moga field," Journal of Petroleum Exploration and Production Technology, vol. 8, pp. 521–529, 6 2017.

[10] D. E. Cannon, "Evaluation of shaly sands with low deliverability," Journal of Canadian Petroleum Technology, vol. 14, 1 1975.

[11] K. D. Luff, "Intelligent computing system for reservoir analysis and risk assessment of the red river formation," 9 2002.

[12] J. Maxwell, P. Ortoleva, D. Payne, and W. Sibo, "Naturally fractured tight gas - gas reservoir detection optimization. quarterly report, june 1, 1996–september 30, 1996," 11 1996.

[13] G. Beardsmore, "The influence of basement on surface heat flow in the cooper basin," Exploration Geophysics, vol. 35, pp. 223–235, 12 2004.

[14] P. A. Aziz and T. Ariadji, "Optimization of horizontal well direction and length considering geomechanics properties and drainage area using genetic algorithm in a gas field," Modern Applied Science, vol. 11, pp. 114–, 8 2017.

[15] A. E. Radwan, "Drilling in complex pore pressure regimes: Analysis of wellbore stability applying the depth of failure approach," Energies, vol. 15, pp. 7872–7872, 10 2022.

[16] M. N. Acharya, M. R. Kabir, S. H. Al-Ajmi, N. A. Al-Maia, A. Kumar, S. P. Pradhan, and E. H. Al-anzi, "Integrated approach to unconventional reservoir characterization: Key for understanding hydrocarbon production challenges in kerogen and tight-fractured deep carbonate complex in kuwait," in SPE Annual Technical Conference and Exhibition, SPE, 10 2012.

[17] D. Wheller, D. G. Selvaggi, K. Kostas, R. Loro, and D. Hearty, "Maximizing production and extending economic life of the woollybutt field: "from little things, big things grow"," in SPE Asia Pacific Oil and Gas Conference and Exhibition, SPE, 10 2010.

[18] S. Wengerd, "Western paradox basin is a potential oil giant in pennsylvanian rocks. pt. 3," Oil & Gas Journal, 2 1970.

[19] E. Hewlett, M. Erickson, C. Ferguson, P. Sherwood, B. Boswell, K. Walter, and M. Hart, "Commercial production of ethanol in the san luis valley, colorado. final report," 7 1983.

[20] B. Gunawan and N. R. Permana, "2d inversion modeling of oil and gas basins using gravity data in tambelang district," JGE (Jurnal Geofisika Eksplorasi), vol. 10, pp. 150–161, 7 2024.

[21] D. Handyside and W. Chipman, "A preliminary study of the hibernia field," Journal of Canadian Petroleum Technology, vol. 22, 5 1983.

[22] J. Park and J. Lee, "Development of designing and performing procedure for well test in coalbed methane(cbm) reservoir," Economic and Environmental Geology, vol. 46, pp. 279–289, 8 2013.

[23] A. Khairunnisa, "Analisa pressure build up dan deliverability dari hasil drill stem test," 12 2018.

[24] H. B. Dhia, "Tunisian geothermal data from oil wells," Geophysics, vol. 53, pp. 1479–1487, 11 1988.

[25] L. Maier, "Recent developments in the interpretation and application of dst data," Journal of Petroleum Technology, vol. 14, pp. 1213–1222, 11 1962.

[26] J. East, "A new system of tools for better control and interpretation of drill stem tests," The APPEA Journal, vol. 9, pp. 153–161, 6 1969.

[27] F. Dollar, "Drill stem testing with jet pump," in SPE Latin America Petroleum Engineering Conference, SPE, 10 1990.

[28] C. F. Tucker, M. C. Dean, R. C. Pahmiyer, K. Bate, P. D. Omotosho, H. F. F. Walli, Z. Ahmad, and P. L. Brittingham, "Developing offshore tight gas sands and navigating subsurface uncertainty," in International Oil and Gas Conference and Exhibition in China, SPE, 6 2010.

[29] D. Finley and C. Wendier, "Openhole dst of a horizontal well: A case study," in Low Permeability Reservoirs Symposium, SPE, 4 1993.

[30] N. Khan and K. Rehman, "Petrophysical evaluation and fluid substitution modeling for reservoir depiction of jurassic datta formation in the chanda oil field, khyber pakhtunkhwa, northwest pakistan," Journal of Petroleum Exploration and Production Technology, vol. 9, pp. 159–176, 7 2018.

[31] M. Rose, "Nitrogen–an oil field tool," 9 1966.

[32] M. Dunkel, P. A. Leonard, D. Carpenter, and C. Murray, "Wireless transfer successfully transmits bottomhole data during drill-stem testing in a multi-well program offshore gabon," in Offshore Technology Conference, OTC, 5 2003.

[33] D. Hamilton, C. Newton, M. Smyth, T. Gilbert, N. Russell, A. McMinn, and L. T. Etheridge, "The petroleum potential of the gunned ah basin and overlying surat basin sequence, new south wales," The APEA Journal, vol. 28, pp. 218–241, 6 1988.

[34] F. Al-Otaibi, H. Al-Bader, A. Al-Ibrahim, P. Subban, V. S. Duggirala, and M. Ayyavoo, "Successful implementation and effective hydraulic fracturing of jurassic, hpht and tight carbonate reservoir in the state of kuwait: A case study of an exploration well," in SPE International Conference and Exhibition on Formation Damage Control, SPE, 2 2020.

[35] M. Mintha and C. Normann, "Putting acoustic telemetry to the test: Design and execution of a subsea, single trip, triple independent zone dst," in Mediterranean Offshore Conference, SPE, 10 2024.